CDF note 11156

Measurement of the Forward-Backward Asymmetry in Bottom-Quark Pair Production Using Soft Muon

The CDF Collaboration
URL http://www-cdf.fnal.gov
(Dated: March 12, 2015)

We investigate the forward-backward asymmetry, $A_{\rm FB}$, in b-quark pair production in proton-antiproton collision at $\sqrt{s} = 1.96\,\text{GeV}$ with the CDF detector. The soft muon tag technique has been applied to identify $b\bar{b}$ production. Using the full CDF data set ($6.9\,\text{fb}^{-1}$) we have obtained the integrated asymmetry at particle level of $A_{\rm FB}= (1.2 \pm 0.7)\%$ for dijet invariant mass above $40\,\text{GeV}/c^2$. Dependence of $A_{\rm FB}$ on dijet invariant mass has been retrieved.

Preliminary Results for Winter 2015 Conferences

I. INTRODUCTION

The study of forward-backward asymmetry ($A_{\rm FB}$) in quark pair production is of a great importance due to its potential contribution to a solution of the problem of matter-anti matter asymmetry in Universe [1]. Results from the measurement based on the full CDF data set ($9.4\,{\rm fb}^{-1}$) show a sizeable difference between the measured forward-backward asymmetry in $t\bar{t}$ quark pair production and the Standard Model (SM) prediction with the significance between 2σ to 3σ [2]. Furthermore, the results show that the asymmetry rises linearly with the invariant mass of the quark pair $M_{q\bar{q}}$. The results from the D0 measurements are consistent with both, the SM predictions and the CDF results [3]. The study of forward-backward asymmetry in a $b\bar{b}$ pair production might therefore bring more light into the origin of the asymmetry, since it would probe regions of lower invariant mass of quark pair. The measurement of $A_{\rm FB}$ in $b\bar{b}$ pair production at high mass ($M_{b\bar{b}}$>$150\,{\rm GeV}/c^2$) presents results consistent with both, the SM predictions and zero [4]. The study presented in this note investigates $A_{\rm FB}$ in $b\bar{b}$ pair production at low mass.

In the measurement we first estimate the fraction of the $b\bar{b}$ events in the collected data using template fit. Then we unfold the background subtracted asymmetry to the particle-level one. The note is organize as follows. Section II briefly describes origin of the asymmetry in heavy quark pair production and gives the theoretical predictions. In Sec. III, the data sample and event selection are presented. The definition of the asymmetry is described in Sec. IV. The unfolding procedure is discussed in Sec. V. The backgrounds are investigated in Sec. VI. In Sec. VII the systematic uncertainties are presented. The results are presented in Sec. VIII.

II. ORIGIN OF THE ASYMMETRY AND THEORETICAL PREDICTION

The two main Standard Model (SM) strong interaction pair-production channels are $q\bar{q} \to b\bar{b}$ and $gg \to b\bar{b}$, neither of which contribute to A_{FB} in the leading-order (LO) perturbative calculations. However, when higher-order corrections are considered, there are several sources of asymmetry [5–7]. Radiative corrections to quark-antiquark annihilation involve either virtual or real gluon emission, which lead to the asymmstry due to interference of initial-state and final-state radiative gluon diagrams and interference of box diagram with the Born one. Interference of different amplitudes in flavor excitation of $q + g$ processes leads to the asymmetry. There is some contribution from electro-weak (EW) production processes: $q\bar{q} \to Z/\gamma* \to b\bar{b}$. On the other hand no asymmetry is expected in gg processes.

Unlike the top quark pair production at the Tevatron, where the dominant production channel is the $q\bar{q}$ annihilation, in the $b\bar{b}$ pair production the dominant production occurs through gluon-gluon fusion, which does not contribute to $A_{\rm FB}$. As a consequence, when the full cross section is considered (gg, $q\bar{q}$ and qg ($\bar{q}g$) interactions are included), the integrated asymmetry predicted by the SM is small due to a big symmetric gluon contribution. However, it is possible to increase the $q\bar{q} \to b\bar{b}$ fraction by the appropriate selection criteria, which can lead to a sizable forward-backward asymmetry.

There are two sets of the theoretical predictions for the $A_{\rm FB}$ at low mass [8, 9]. Table I presents the prediction of Grinstein and Murphy [9] expressed for bins of $b\bar{b}$ invariant mass, $M_{b\bar{b}}$ similar to our analysis. The prediction is calculated for $b\bar{b}$ pair with maximum acollinearity of $\delta = \pi - 2.8$ rad and requiring b and $\bar{b}$ quarks to have transverse momenta ($p_{{\rm T}b,\bar{b}}$) greater than 15 GeV/c and rapidity [10] of $\mid y_{b,\bar{b}} \mid \leq 1$. In the predictions, near the Z pole, the SM bottom asymmetry is dominated by tree level exchanges of EW gauge bosons.

III. DATA SAMPLE AND EVENT SELECTION

The analysis is based on the full CDF Run II data sample of the integrated luminosity of $6.9{\rm fb}^{-1}$. The data are collected with a central muon trigger that requires an muon with ${\rm p}_T$ >8 GeV/c and pseudorapidity $|\eta| < 0.6$ [11]. From the dataset we select events offline requiring a muon track with p_T > 10 GeV/c inside a jet with ${\rm E}_T$ >20 GeV (this is the so-called muon jet). There should be

$M_{b\bar{b}}$ [GeV/c^2]	$A_{\rm FB}^{b\bar{b}}$ [%]
$[35, 75]$	$0.18 \pm 0.05\ ^{+0.01}_{-0.01}$
$[75, 95]$	$2.84 \pm 0.20\ ^{+0.69}_{-0.58}$
$[95, 130]$	$1.79 \pm 0.37\ ^{+0.24}_{-0.20}$
> 130	$3.52 \pm 1.01\ ^{+0.28}_{-0.24}$
Inclusive	$0.30 \pm 0.07\ ^{+0.04}_{-0.03}$

TABLE I: $A_{\rm FB}$ prediction calculated by Grinstein and Murphy [9]. All parton-level cuts match our analysis cuts except requirement on $p_{{\rm T}b,\bar{b}}$. We require particle-level jets to have $p_{\rm T} > 20$ GeV/c.

another jet back to back ($|\Delta\phi| > 2.8$) with the muon jet that has E$_T$ >20 GeV and $|\eta| < 1.0$ (this is the so-called away jet). The muon and away jets have to be balanced in p_T:

$$p_{T,Bal} = \frac{|p_T^{\mu{\rm J}} - p_T^{\rm AJ}|}{\max\{p_T^{\mu{\rm J}}, p_T^{\rm AJ}\}} < 0.6 \tag{1}$$

where $p_T^{\mu{\rm J}}(p_T^{\rm AJ})$ is transverse momenta of muon (away) jet. In addition to that both jets have to be identified as b jets using tight (loose) version of the secondary vertex algorithm [12] for away (muon) jet.

The simulations rely on the Pythia Monte Carlo dijet sample enriched in heavy flavor (leading order (LO) production is assumed). The $M_{b\bar{b}}$ distribution for $Z - \gamma^*$ production has been modeled by re-weighting events from the Pythia Monte Carlo sample using the ratio of the LO differential cross sections of the QCD and EW processes computed by MadGraph [13]. The 10% asymmetry [14] has been introduced to the modeled $Z - \gamma^*$ distribution.

IV. METHODOLOGY

For the $b\bar{b}$ pair production, one can in principle define two asymmetries – the charge asymmetry and the forward-backward asymmetry. As a consequence of CP conservation assumption in strong interactions the two asymmetries are equal.

The integrated forward-backward asymmetry can be expressed using the difference of rapidities of the b and $\bar{b}$ quark, Δy_b. The advantage of this approach is, that Δy_b is invariant under Lorentz boost along the beam axis, thus it is the same in both $p\bar{p}$ frame as well as $q\bar{q}$ rest frame. For a b quark from the $b\bar{b}$ pair moving in the forward direction $\Delta y_b > 0$, and for backward direction $\Delta y_b < 0$. The $A_{\rm FB}$ in terms of Δy_b is defined as follows:

$$A_{\rm FB} = \frac{N(\Delta y_b > 0) - N(\Delta y_b < 0)}{N(\Delta y_b > 0) + N(\Delta y_b < 0)} \tag{2}$$

In the case of dijet events, where one of the jets contain a muon (our data selection), the Δy_b variable is defined as follows:

$$\Delta y_b = Q(\mu)(y_{AJ} - y_{\mu J}) \tag{3}$$

where $Q(\mu)$ is the charge of the muon and $y_{\rm AJ}$ or $y_{\mu{\rm J}}$ is the rapidity of the away or muon jet, respectively.

V. UNFOLDING PROCEDURE

The goal is to measure the forward-backward asymmetry, $A_{\rm FB}$, in $b\bar{b}$ production at particle level. To retrieve the true particle level $A_{\rm FB}$, the background has to be subtracted from the reconstructed

(measured) distributions and limited acceptance of the CDF detector and bin-by-bin smearing have to be taken into account. As the Δy_b sign depends on the charge of the muon, a correction for events where cascade decays and $B_0 - \bar{B}_0$ mixing occurs, has to be done. This correction is included in the unfolding procedure.

The measured signal distribution $\vec{b}$ (after background subtraction) is related to the underlying particle-level distribution, $\vec{x}$, by the relation:

$$\vec{b} = \mathbf{S}\mathbf{A}\vec{x}\,. \tag{4}$$

Here, $\mathbf{A}$ is a diagonal matrix, which describes the acceptance in each bin of the measured distribution. The non-diagonal smearing matrix $\mathbf{S}$ describes the migration of events between bins due to a finite resolution of the CDF detector and our reconstruction technique.

The binned data is multiplied by the inverse matrices to recover the true particle-level distribution from the background-subtracted one:

$$\vec{x} = \mathbf{A}^{-1}\mathbf{S}^{-1}\vec{b}\,. \tag{5}$$

Before applying the acceptance correction, we must first remove the resolution smearing from the distribution. To unfold the distribution using the $\mathbf{S}$ matrix an algorithm based on the singular value decomposition (SVD) method [15] is used.

For our analysis, we use the unfolding algorithm implemented in the ROOT package RooUnfold [16]. Ignoring the acceptance matrix, one can write:

$$\vec{b} = \mathbf{S}\vec{x} \tag{6}$$

The SVD algorithm decomposes the non-diagonal response matrix $\mathbf{S}$ into $\mathbf{S} = \mathbf{U}\mathbf{S}'\mathbf{V}^T$, where $\mathbf{U}$, $\mathbf{V}$ are orthogonal matrices, and $\mathbf{S}'$ is a diagonal matrix containing only non-negative entries along the diagonal. The entries of $\mathbf{S}'$ are called singular values of $\mathbf{S}$. The unfolding procedure is then reduced to the inversion of a diagonal matrix.

The pure inversion of the matrix $\mathbf{S}'$ would lead to problems if large statistical fluctuations are present. To avoid these problems an *a priori* chosen regularization condition is needed. One can look at the unfolding problem as at a least-squares minimization of the expresion

$$(\mathbf{S}\vec{x} - \vec{b})^T\mathbf{B}^{-1}(\mathbf{S}\vec{x} - \vec{b})\,, \tag{7}$$

where $\mathbf{B}$ is the covariance matrix of $\vec{b}$.

The *a priori* chosen regularization condition is then added to this minimization:

$$(\mathbf{S}\vec{x} - \vec{b})^T\mathbf{B}^{-1}(\mathbf{S}\vec{x} - \vec{b}) + \tau(\mathbf{C}\vec{x})^T(\mathbf{C}\vec{x}), \tag{8}$$

where $\mathbf{C}$ defines the regularization condition, and the τ determines relative strength given to this condition. We use the regularization condition chosen in [15], which maximizes the "smoothness" of the unfolded distribution by minimizing the second derivative. This is imposed by the matrix $\mathbf{C}$:

$$C = \begin{pmatrix} -1 & 1 & 0 & 0 & \dots & 0 \\ 1 & -2 & 1 & 0 & \dots & 0 \\ 0 & 1 & -2 & 1 & \dots & 0 \\ \dots & \dots & \dots & \dots & \dots & \dots \\ 0 & \dots & 0 & 1 & -2 & 1 \\ 0 & \dots & 0 & 0 & 1 & -1 \end{pmatrix} \tag{9}$$

The optimal regularization strength τ is related to the singular value of response matrix **S**. If the singular values s_i are listed by decreasing absolute value, there is some value s_k such that the optimal τ is given by $\tau = s_k^2$. The index k is the regularization parameter used as input into the RooUnfold algorithm. For very large k, the SVD unfolding is equivalent to the pure matrix inversion. For very small k, the regularization condition is strongly enforced. If $k = 0$, the unfolded histogram is equivalent to the distribution used to create the response matrix, regardless of the measured distribution used as input.

A. Inputs for unfolding

To measure the $A_{\rm FB}$ at the particle level as a function of $M_{b\bar{b}}$, we need to unfold $M_{b\bar{b}}$ and Δy_b distributions. To be able to do one dimensional (1D) unfolding we define a distribution of events divided into eight bins:

- two Δy_b-bins: positive and negative Δy_b,
- four $M_{b\bar{b}}$-bins: $[40, 75]$, $[75, 95]$, $[95, 130]$, and $[130, \infty]$,

as is shown at Fig. 1.

To define the $M_{b\bar{b}}$ and Δy_b distributions at particle level, we are looking for a muon-away jet pair at the particle level. The particle-level jets and muon have to pass same selection criteria as those at the reconstruction level (Sec. III). To be able to define true Δy_b we require muon and away jets at particle level to be matched with opposite sign b quarks using Monte Carlo true information.

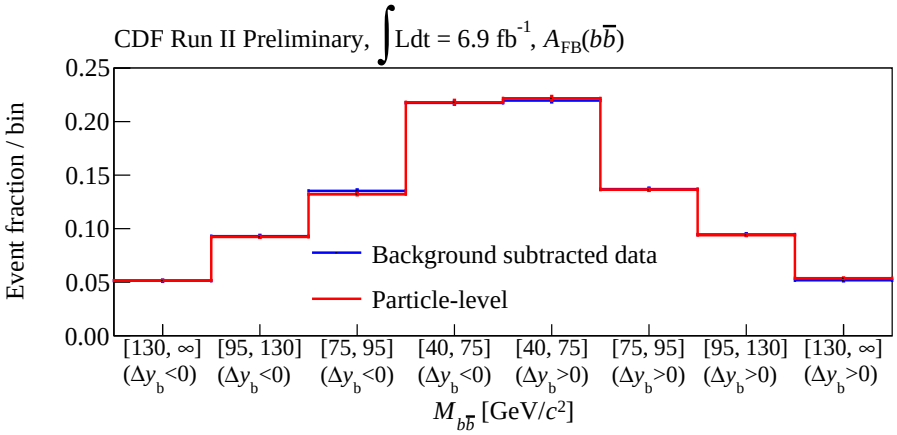

FIG. 1: The background subtracted distribution (blue) corresponds to the input of the used unfolding procedure. The particle-level distribution (red) corresponds to the output of the unfolding procedure.

B. Smearing and acceptance matrices

Due to finite resolution of the CDF detector we define matrix of bin-to-bin smearing. The matrix expresses the probability of measuring the true (particle-level) $M_{b\bar{b}}^{\rm true}$ in a reconstructed (detector-level) $M_{b\bar{b}}$ bin. Fig. 2 shows our smearing matrix used in the unfolding procedure.

The smearing matrix is diagonal, with some anti-diagonal terms. The anti-diagonal terms come from events where the electric-charge sign of the muon is changed due to the $B_0 - \bar{B}_0$ mixing or cascade $b \to c \to \mu$ decays. The muon sign is used to express the measured Δy_b. To prove this

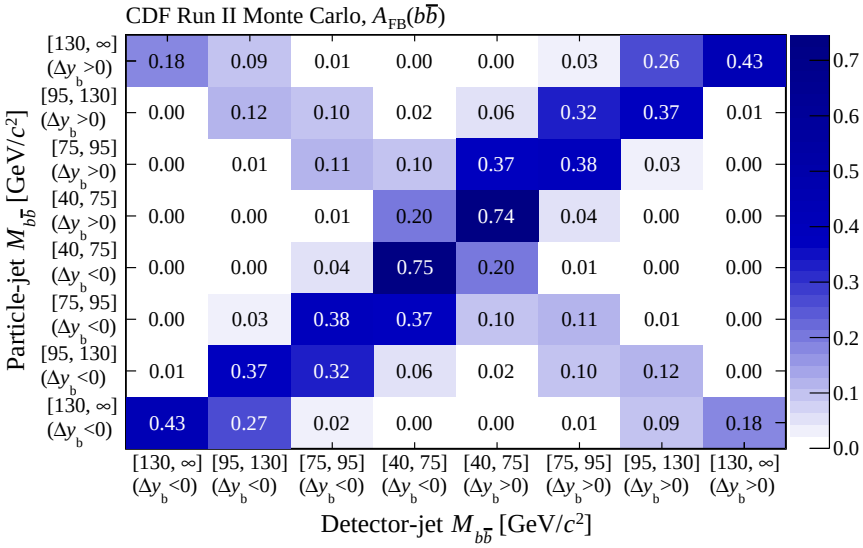

FIG. 2: Smearing matrix - all events. Used in the unfolding procedure.

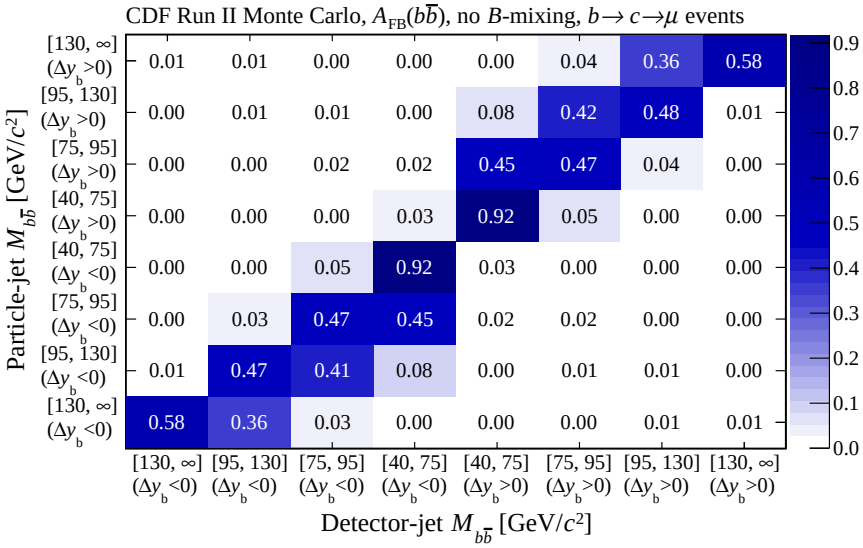

FIG. 3: Smearing matrix - no cascade decays and $B_0 - \bar{B}_0$ mixing events.

hypothesis, we present the smearing matrix defined on "pure" events (Fig. 3), where no $B_0 - \bar{B}_0$ mixing and cascade $b \to c \to \mu$ decays occurred.

The acceptance matrix is a diagonal matrix, which express how many events pass our detector-level selection criteria.

The smearing and acceptance matrices are modeled using the PYTHIA Monte Carlo sample together with the modeled $Z - \gamma^*$ production of $b\bar{b}$ events.

C. Optimization of regularization parameter k

In the unfolded distribution the $M_{b\bar{b}}$ bins $[40; 75]\,\mathrm{GeV}/c^2$ and $[130; \infty]\,\mathrm{GeV}/c^2$ are considered as the "edge" bins. Therefore the corresponding elements of $\mathbf{C}$ are $-1+\xi$ rather than $-2+\xi$. For the unfolding procedure we then use curvature matrix defined as follows:

$$C = \begin{pmatrix} -1+\xi & 1 & 0 & 0 & 0 & 0 & 0 & 0 \\ 1 & -2+\xi & 1 & 0 & 0 & 0 & 0 & 0 \\ 0 & 1 & -2+\xi & 1 & 0 & 0 & 0 & 0 \\ 0 & 0 & 1 & -1+\xi & 0 & 0 & 0 & 0 \\ 0 & 0 & 0 & 0 & -1+\xi & 1 & 0 & 0 \\ 0 & 0 & 0 & 0 & 1 & -2+\xi & 1 & 0 \\ 0 & 0 & 0 & 0 & 0 & 1 & -2+\xi & 1 \\ 0 & 0 & 0 & 0 & 0 & 0 & 1 & -1+\xi \end{pmatrix} \tag{10}$$

where $\xi = 0.00001$.

To find the best value of the regularization parameter k we have introduced an asymmetry into our PYTHIA MC sample by re-weighting the selected events. For each $M_{b\bar{b}}$ bin several introduced asymmetries around the predicted asymmetry has been tested by running 1000 pseudo-experiments (PEs) for each regularization parameter k. The asymmetry after unfolding procedure has been compared with the true introduced asymmetry. From the comparison of the results the $k = 4$ has been chosen as the optimal regularization parameter.

VI. BACKGROUND

There are four sources of the background events. The $c\bar{c}$ events are mainly produced via symmetric gluon-gluon fusion. The events where one of the jets has been initiated by b quark, while the other by c quark are produced via gluon-quark interactions, which give a small contribution into the asymmetry. The asymmetry contribution from the events with at least one light jet, which has been mis-tagged as b-jet, has been using data driven technique. The obtained asymmetries are consistent with zero within their uncertainties. In case of the events with the fake muons, no asymmetry is expected, as direction of the fake-muon trajectory has constant distribution. Therefore the background is treated as symmetric.

To obtain the fraction of true $b\bar{b}$ events, $f_{b\bar{b}}$, in data, the b fractions on muon- and away-jet sides have been determined using two template fits.

In order to the extract the b content on the muon-jet side, we use the $p_{\mathrm{T,rel}}$ distribution of muon with respect to the jet axis, which tends to peak at larger values when the muon is coming from a b jet than when it is coming from a c or light quark jet. The templates for the c or light quark jets are very similar so we do a two template fit to get the fraction of cases with the muon coming from a b jet. For the away-jet side we do another template fit using the secondary vertex mass distribution of the away jet, which shows that as the incoming quark mass is higher, the secondary vertex mass distribution tends to peak at higher values. In this case we also perform a two template fits. The templates are shown in Figures 4 and 5 as a function of dijet invariant mass M_{jj}. Figures 6 and 7 show the examples of the fits of the $p_{\mathrm{T,rel}}$ and M_{vtx} distributions for M_{jj} bin of $[95; 130]\,\mathrm{GeV}/c^2$, respectively.

We obtain the $b\bar{b}$ fraction in each M_{jj} bin by computing the average b fraction between its lowest and highest value. The highest value is the maximum of the b fractions obtained for muon- and away-jet side. The lowest value is obtained by subtracting from the highest value the maximum of the non-b fractions determined for the muon- and away-jet side. The uncertainty on the average value covers the difference with the highest and lowest value. The results are shown at Fig. 8. The systematic uncertainties coming from the fit strategy and template shapes for M_{jj} bins are summarized in Tab. II.

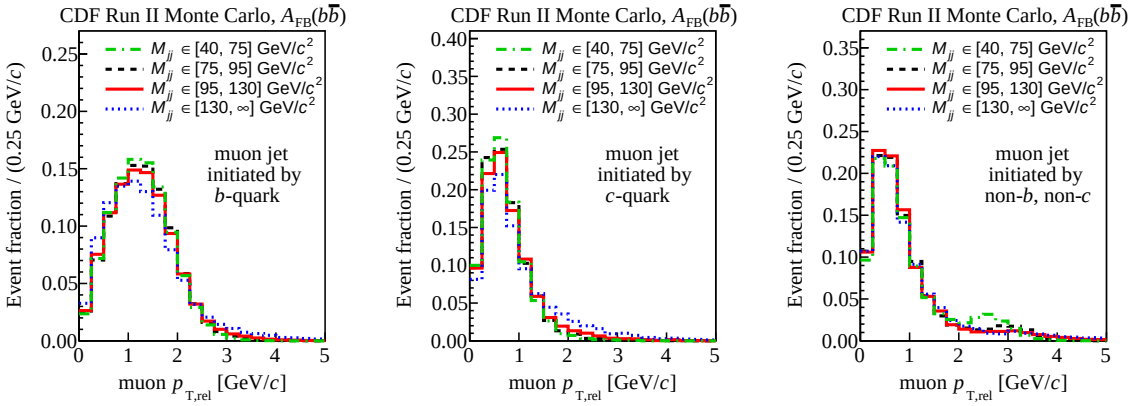

FIG. 4: $p_{\mathrm{T,rel}}$ MC templates for the b-tagged jets on muon jet side initiated by b-, c-quark, and light quark (or gluon) as a function of dijet invariant mass M_{jj}.

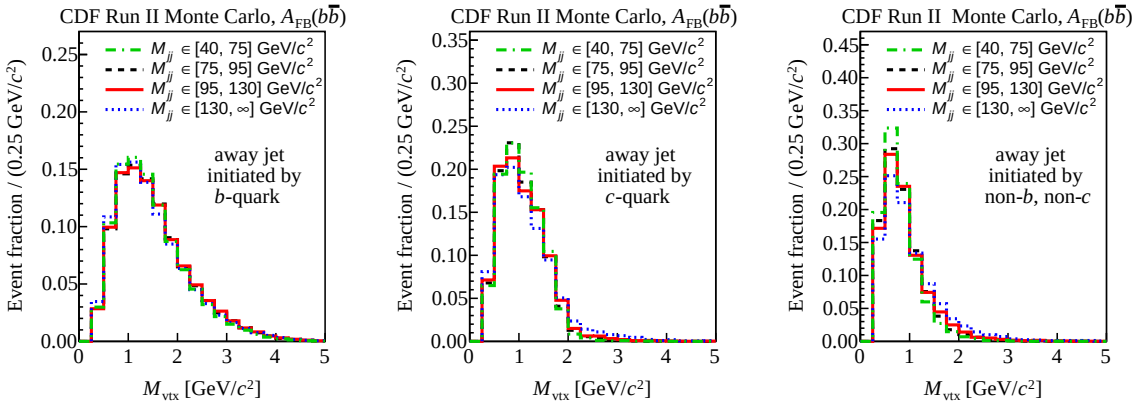

FIG. 5: M_{vtx} MC templates for the b-tagged jets on away jet side initiated by b-, c-quark, and light quark (or gluon) as a function of dijet invariant mass M_{jj}.

TABLE II: Systematic uncertainties related to the procedure used to find $f_{b\bar{b}}$ fraction in data.
CDF Run II Preliminary, $\int \mathrm{Ldt} = 6.9\,\mathrm{fb}^{-1}$, $A_{\mathrm{FB}}(b\bar{b})$

Absolute uncertainty of $f_{b\bar{b}}$ [%]				
Source	M_{jj} [GeV/c^2]			
	[40; 75]	[75; 95]	[95; 130]	[130; ∞]
fit strategy	1.6	0.8	2.2	1.3
template shape	3.5	3.3	6.4	8.7
total syst.	3.8	3.4	6.8	8.8
stat.	1.5	2.6	4.1	6.0
total	4.1	4.3	7.9	10.7

VII. SYSTEMATIC UNCERTAINTIES

Systematic uncertainties in this analysis come from MC modeling of the geometrical and kinematic acceptance, estimation of the amount of the background events, and possible background asymmetry.

Monte Carlo modeling of geometrical and kinematic acceptance include effects of initial and final

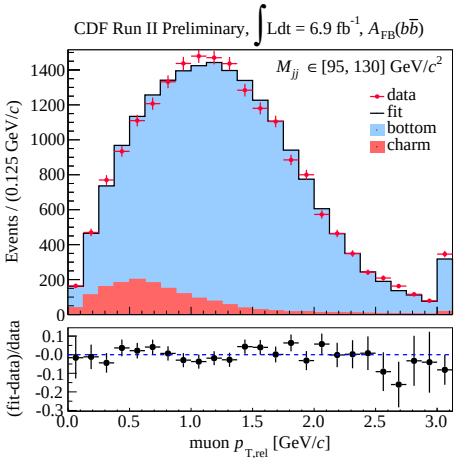

FIG. 6: The result of the two component fit of $p_{\mathrm{T,rel}}$ distribution for M_{jj} of $[95; 130]\,\mathrm{GeV}/c^2$.

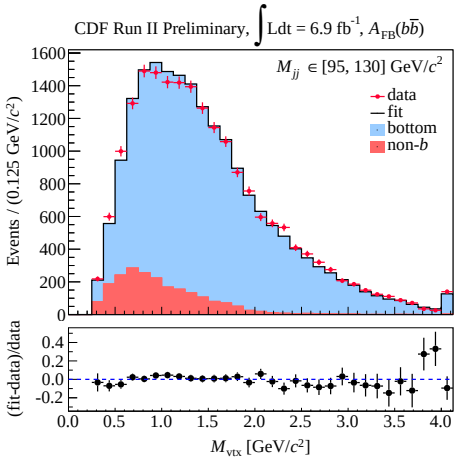

FIG. 7: The result of the two component fit of M_{vtx} distribution for M_{jj} of $[95; 130]\,\mathrm{GeV}/c^2$

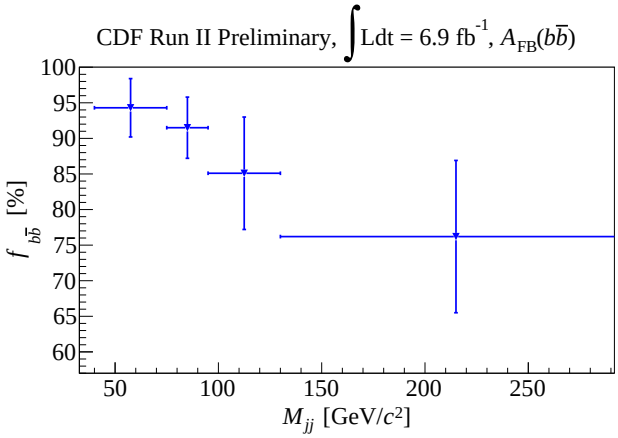

FIG. 8: The $b\bar{b}$ fractions obtained from data. The uncertainties include the statistical and systematic uncertainties.

state radiation (ISR and FSR), and jet energy scale. These are estimated by varying ISR, FSR and the jet energy scale in the Monte Carlo. The uncertainty due to the amount of background is estimated by varying the obtained $b\bar{b}$ fraction within its uncertainty. The systematic uncertainty due to possible background asymmetry is estimated by inserting $\pm 1\%$ asymmetry into the background distribution. The total systematic uncertainties for different $M_{b\bar{b}}$ bins are summarized in Tab. III.

VIII. RESULTS

Following the procedure described in the previous sections, the forward-backward asymmetry is expressed at three levels: reconstructed (raw), after background subtraction and at particle level. The results are summarized in Tab. IV. The A_{FB} dependence on $M_{b\bar{b}}$ and the integrated asymmetry are presented.

Figure 1 shows the input (background-subtracted distribution) and output (particle-level distribution) of the used unfolding procedure. The final results, which includes also systematic uncertainties, are summarized in Tab. V. Figure 9 shows comparison of the measured results with the theoretical

TABLE III: Systematic uncertainties.
CDF Run II Preliminary, $\int$Ldt $= 6.9\,\text{fb}^{-1}$, $A_{\text{FB}}(b\bar{b})$

Absolute uncertainty of A_{FB} [%]					
	$M_{b\bar{b}}$ [GeV/c^2]				Integrated
	$[40;75]$	$[75;95]$	$[95;130]$	$[130;\infty]$	
$f_{b\bar{b}}$ uncert.	0.06	0.06	0.04	0.01	0.04
Background A_{FB}	0.11	0.17	0.27	0.34	0.17
JES	0.24	0.15	0.02	0.10	0.10
ISR/FSR	0.09	0.07	0.06	0.12	0.05
total	0.29	0.24	0.28	0.37	0.22

prediction, which are calculated at the parton level using a different lower threshold for the lowest $M_{b\bar{b}}$ bin. The measured particle-level distribution shows a tendency of the A_{FB} asymmetry to increase with $M_{b\bar{b}}$ with a spike around Z pole mass similar to the theoretical prediction. The measured integrated asymmetry of $(1.2 \pm 0.7)\%$ is consistent with the prediction.

TABLE IV: The results of the A_{FB} measurements at three levels. The uncertainties are statisitcal only.
CDF Run II Preliminary, $\int$Ldt $= 6.9\,\text{fb}^{-1}$, $A_{\text{FB}}(b\bar{b})$

	$A_{\text{FB}}(b\bar{b})$ [%], statistical uncertainties only				
	M_{jj} [GeV/c^2]				Integrated
	$[40;75]$	$[75;95]$	$[95;130]$	$[130;\infty]$	
detector level	0.47 ± 0.49	0.55 ± 0.61	0.70 ± 0.71	0.32 ± 0.91	0.52 ± 0.32
bckg subtr.	0.50 ± 0.54	0.60 ± 0.70	0.83 ± 0.90	0.43 ± 1.33	0.58 ± 0.37
particle level	0.83 ± 0.83	1.54 ± 0.69	0.92 ± 0.82	2.08 ± 1.03	1.17 ± 0.68

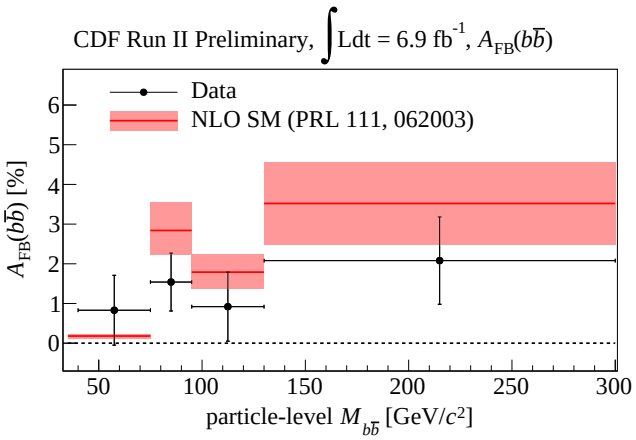

FIG. 9: Measured A_{FB} as a function of particle-level $M_{b\bar{b}}$. The data are compared with the theoretical prediction.

TABLE V: The final results of the A_{FB} measurements including systematic uncertainties.
CDF Run II Preliminary, $\int$Ldt $= 6.9\,\text{fb}^{-1}$, $A_{\text{FB}}(b\bar{b})$

	$M_{b\bar{b}}$ [GeV/c^2]				Integrated
	$[40;75]$	$[75;95]$	$[95;130]$	$[130;\infty]$	
particle level	0.83 ± 0.88	1.54 ± 0.73	0.92 ± 0.87	2.08 ± 1.10	1.17 ± 0.71

Acknowledgments

We thank the Fermilab staff and the technical staffs of the participating institutions for their vital contributions. This work was supported by the U.S. Department of Energy and National Science Foundation; the Italian Istituto Nazionale di Fisica Nucleare; the Ministry of Education, Culture, Sports, Science and Technology of Japan; the Natural Sciences and Engineering Research Council of Canada; the National Science Council of the Republic of China; the Swiss National Science Foundation; the A.P. Sloan Foundation; the Bundesministerium für Bildung und Forschung, Germany; the Korean Science and Engineering Foundation and the Korean Research Foundation; the Science and Technology Facilities Council and the Royal Society, United Kingdom; the Russian Foundation for Basic Research; the Comisión Interministerial de Ciencia y Tecnología, Spain; the Slovak R&D Agency; and the Academy of Finland; and the Australian Research Council (ARC).

---

[1] M. Shaposhnikov, Prog. Theor. Phys. (2009) 122: 185-203.
[2] Measurement of the top quark forward-backward production asymmetry and its dependence on event kinematic properties., T. Aaltonen *et al.* (CDF Collaboration), Phys. Rev. **D** 87, 092002 (2013).
[3] Measurement of the forward-backward asymmetry in top quark-antiquark production in $p\bar{p}$ collisions using the lepton+jets channel, V.M. Abazov *et al.* (The D0 Collaboration), Phys. Rev. **D** 90, 072011 (2014).
[4] Forward-backward asymmetry in $b\bar{b}$ pairs at high mass, CDF Conf Note 11092.
[5] J.H. Khun and G. Rodrigo, Phys. Rev. Lett. 81 (1998) 49.
[6] J.H. Khun and G. Rodrigo, Phys. Rev. **D**59, 054017 (1999).
[7] W. Bernreuter,et al. arXive: hep-ph/0604031v1.
[8] Forward-backward and charge asymmetries at Tevatron and LHC, G. Rodrigo, CKM 2014, Vienna, Austria, Sep 11, 2014.
[9] B. Grinstein, Ch. W. Murphy, Phys. Rev. Lett. 111, 062003 (2013).
[10] Rapidity is defined as $y = -\frac{1}{2}\ln\frac{E+p_z}{E-p_z}$, where E is particle's energy and p_z is its momenta component parallel to the beam pipe.
[11] Pseudorapidity is defined as $\eta = -\ln\tan(\theta/2)$, where θ is particle azimuthal angle with respect to the beam pipe.
[12] D. Acosta *et al.* (CDF Collaboration), Phys. Rev. **D**71, 052003 (2005).
[13] Private e-mail communication with Ch. W. Murphy.
[14] Determination of A_{FB}^b at the Z pole using inclusive charge reconstruction and lifetime tagging, J. Abdallah *et al.* (DELPHI Collaboration), Eur.Phys.J. **C** 40, 1-25 (2005).
[15] A. Höcker and V. Kartvelishvili, NIM A **372**, 469 (1996).
[16] T. Adye, RooUnfold Software Package. hepunx.rl.ac.uk/adye/softward/unfold/RooUnfold.html